

Investigation of Cycling Performance in a Solid-State Fluoride-Ion Battery Based on Copper Fluoride Electrodes

Chien-Hung Chen*, Ching-Tsung Yu, Yu-Fei Chang

Department of Chemistry, National Atomic Research Institute, Taoyuan, Taiwan, ROC

Received 22 January 2024; received in revised form 23 April 2024; accepted 24 April 2024

DOI: <https://doi.org/10.46604/ijeti.2024.13297>

Abstract

This study investigates the performance and cycling fading of a solid-state fluoride-ion battery (FIB) based on the CuF₂ electrode. The cathode and solid electrolyte of CuF₂ composite and La_{0.9}Ba_{0.1}F_{2.9} are prepared by ball-milling. Meanwhile, the anode materials are used as Sn and Pb. All FIB cells with sandwich structures are fabricated by compressing under a pressure of 4.5 tons/cm². Electrochemical measurements of discharge/charge are performed at 423 K and under 40 μA/cm². The resultant cycling stability of the cell with the Pb anode is higher than that of the cell with the Sn anode. Concerning the cell with Pb anode, the first and tenth discharge capacities of 150 and 90 mAh/g are obtained. X-ray photoelectron analysis demonstrates that the cycling fading of the cell with the Sn (or Pb) anode may be attributed to the irreversible formation of materials (e.g., SnF₄ or PbF₄) during the electrochemical reaction.

Keywords: fluoride-ion battery, copper fluoride, cycling performance, solid-state battery

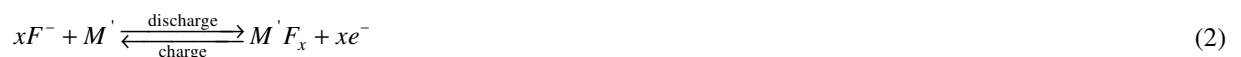
1. Introduction

New secondary battery technologies have attracted significant attention due to the increasing demand for energy storage devices [1]. High energy density and safe rechargeable properties are important in the rapid development of mobile vehicles, electronic devices, and stationary energy storage systems [2-3]. Fluoride ions, characterized by their small ionic size and high electronegativity, are expected to be exceptional anionic conductors [4-5]. High theoretical capacities (approximately 5000 Wh/L) are expected in fluoride-ion battery (FIB) systems, and such an expectation is ascribed to the enablement of metals to form bivalent or trivalent metal fluorides [6]. Reddy and Fichtner [7] first demonstrated a reversible electrochemical reaction in solid-state FIB using a tysonite-type La_{0.9}Ba_{0.1}F_{2.9} electrolyte. The electrochemical principles of FIB are listed as follows [7].

Cathode reaction:



Anode reaction:



where M and M' are cathodic and anodic metal species, respectively.

Regarding solid-state electrolyte material, the tysonite-type La_{1-x}Ba_xF_{3-x} ($0 \leq x \leq 0.15$) is particularly eligible considering large electrochemical stability windows (ESWs) per se [8]. Reddy and Fichtner [7] reported that the ionic conductivity of 1.6×10^{-4} S/cm was measured at 433 K for La_{0.9}Ba_{0.1}F_{2.9} material. La_{0.9}Ba_{0.1}F_{2.9} synthesis methods, including high-energy ball

* Corresponding author. E-mail address: chchen1120@nari.org.tw

milling [9], coprecipitation [10], and sol-gel synthesis [6], have been established. The ionic conductivities were 10^{-4} – 10^{-5} S/cm at 373–473 K. Unfortunately, however, the high activation energy of 0.5–0.6 eV for $\text{La}_{0.9}\text{Ba}_{0.1}\text{F}_{2.9}$ exhibited low ionic conductivity under room temperature conditions [11]. Notably, given the reduction in grain boundaries, the conductivity of $\text{La}_{0.9}\text{Ba}_{0.1}\text{F}_{2.9}$ was efficiently improved by sintering at high temperatures [9]. In addition, MSnF_4 (M = Ba and Pb) materials [12] evince sufficient ionic conductivity (10^{-3} – 10^{-4} S/cm) under room temperature. Nevertheless, the narrow ESWs properties of MSnF_4 significantly limited the cell voltage (approximately 0.5 V) [13].

In addition to solid-state electrolytes, the electrode material is also crucial in the performance of FIB. The theoretical capacity of FIB cells strongly depends on the active material species. Potential active materials for cathodes involving BiF_3 [11], CuF_2 [14], SnF_2 [7], KBiF_4 [7], and $\text{La}_2\text{NiO}_{4+d}$ [15] have been discussed previously. On the other hand, anode materials such as Ce [10], La [14], Pb [13], Mg [16], Sn [4], and Zn [8] are introduced herein. These results indicate that cycling performance is a technical challenge. Several factors affecting cycling have been reported, including significant volume changes in the active material during discharge/charge cycling [1, 16], irreversible impurity formation [14], conductive resistance [16], and electrode/electrolyte interface contact [7]. More detailed characterization should be further clarified to improve the cycling performance of FIB.

This study aims to investigate the development of innovative materials such as $\beta\text{-KSnF}_4$ [17] and KSn_2F_5 [18] for solid-state electrolytes to achieve ionic conductivity of 10^{-4} S/cm at room temperature. However, the cycling fading of anode materials for FIB is currently constrained. In this study, CuF_2 was deployed as the active material in the cathode because of its high theoretical capacity of 527 mAh/g. The solid electrolyte of tysonite-type $\text{La}_{0.9}\text{Ba}_{0.1}\text{F}_{2.9}$ was used. Two common metals, Sn and Pb, were selected as anode materials. The cycling performances of the solid-state FIB cells were evaluated at 423 K and under $40 \mu\text{A}/\text{cm}^2$. Furthermore, the cycling fading of FIB cells was examined by an X-ray photoelectron spectroscopy (XPS) to understand the fading mechanism of FIB cells.

2. Experiments

The performance of solid-state FIB based on a CuF_2 electrode was investigated in this study. The cathode and solid electrolyte were employed to be CuF_2 composite and $\text{La}_{0.9}\text{Ba}_{0.1}\text{F}_{2.9}$, respectively. On the other hand, the anode materials were tested using either Sn or Pb. The detailed experimental description is outlined as follows.

2.1. Preparation of electrolyte and electrode

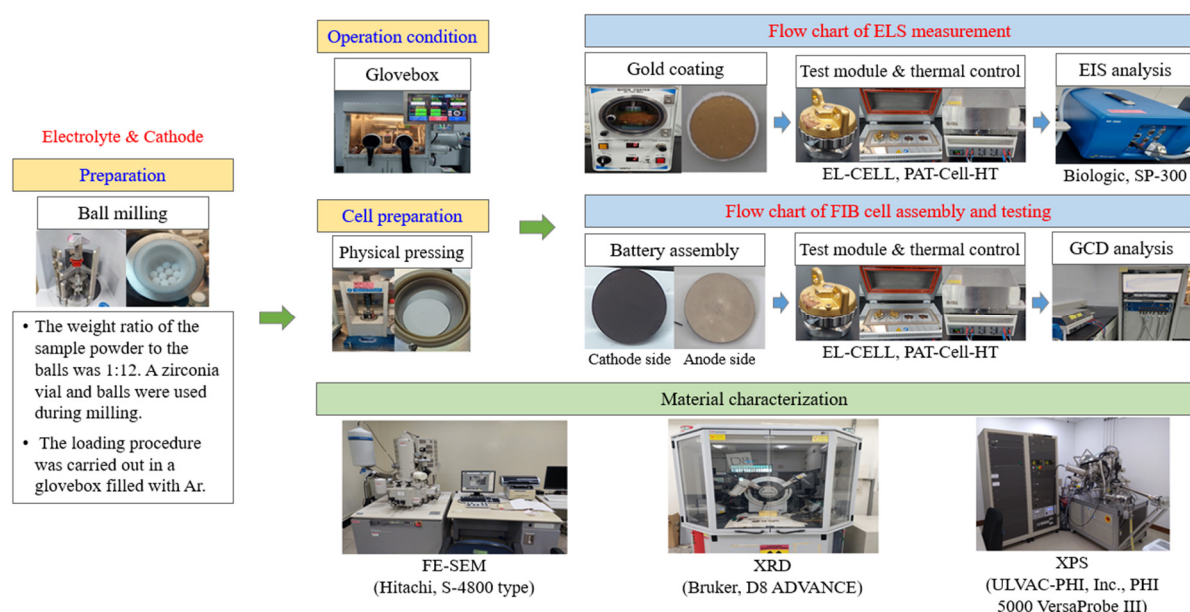


Fig. 1 Flow chart of FIB experiments in this study

Fig. 1 depicts a flow chart of FIB experiments in this study. The solid electrolyte, $\text{La}_{0.9}\text{Ba}_{0.1}\text{F}_{2.9}$, was synthesized using a mechanical ball-milling method. A stoichiometric mixture of lanthanum(III) fluoride (LaF_3 , Sigma Aldrich, 99.9%) and barium fluoride (BaF_2 , Sigma Aldrich, 99.9%) was milled at 600 rpm for 12 hours. The weight ratio of the sample powder to the balls was 1:12. During milling, a zirconia vial and balls were used. The loading procedure of the powders and balls into the milling vial was carried out in a glovebox filled with argon. Apropos the cathode materials, the composite was prepared by the mixture of copper fluoride (CuF_2 , Sigma Aldrich, 99.9%), carbon black (Super P, Alfa Aesar, 99%), and $\text{La}_{0.9}\text{Ba}_{0.1}\text{F}_{2.9}$ in a weight ratio of 30:10:60. The cathode mixture was milled at 600 rpm for 12 hours. The weight ratio of the powder mixture to the balls was 1:16. Moreover, nanometal Sn (< 150 nm, Sigma Aldrich, 99%) and Pb foil were used as anode materials herein.

2.2. Electrochemical measurement

The electrochemical impedance spectroscopy (EIS, Biologic, SP-300) measurements of the $\text{La}_{0.9}\text{Ba}_{0.1}\text{F}_{2.9}$ solid electrolyte were performed in the frequency range of 7 MHz to 1 Hz. A voltage with an amplitude of 10 mV was applied. The EIS spectra were collected at a temperature range from 298 K to 443 K. The EIS samples were prepared by compressing (4.5 ton/cm^2) to form a pellet (13 mm diameter, and approximately 0.6 mm thickness) and coated with gold on both sides as ion-blocking electrodes. The ionic conductivity of $\text{La}_{0.9}\text{Ba}_{0.1}\text{F}_{2.9}$ electrolyte was calculated as follows [3]:

$$\sigma_{DC} = \frac{l}{A} \times \frac{1}{R} \quad (3)$$

where σ_{DC} is the ionic conductivity (S/cm), l represents the pellet thickness of the electrolyte, R denotes the resistance of the electrolyte, and A symbolizes the pellet area.

According to the Arrhenius law, the activation energy can be calculated [5]:

$$\sigma_{DC} = \frac{\sigma_0}{T} \exp\left(-\frac{E_a}{kT}\right) \quad (4)$$

$$\ln(\sigma_{DC} T) = \ln \sigma_0 - \frac{E_a}{kT} \quad (5)$$

where E_a is the activation energy (eV), k is the Boltzmann constant (8.617×10^{-5} eV/K), T is the temperature (K), and σ_0 is the preexponential factor.

2.3. Battery assembly and testing

The solid-state cell samples, which comprise a cathode mixture layer, a $\text{La}_{0.9}\text{Ba}_{0.1}\text{F}_{2.9}$ electrolyte layer, and an anode layer, were assembled by compressing under a pressure of 4.5 tons/cm^2 . Moreover, the weight ratio of the cathode, electrolyte, and anode was 1:95:5. The prepared cell sample was subsequently introduced into a commercial test cell (EL-CELL, PAT-Cell-HT), and the cell assemblies were performed in a glove box under an argon atmosphere. Galvanostatic charge-discharge (GCD) experiments were performed at 423 K and under $40 \mu\text{A/cm}^2$, using a charge-discharge instrument (Biologic, BCS-805). The cut-off voltages of discharge and charge at 423 K were 0.05 V and 1.7 V, respectively.

2.4. Material characterization

The electrolyte materials were characterized by X-ray diffraction (XRD, Bruker, and D8 ADVANCE with a Cu $K\alpha$ radiation source), whose experiments were performed in the 2θ range of 23° to 29° and 42° to 46° . The structures and morphologies of the materials were observed using a field-emission scanning electron microscope (FE-SEM, Hitachi, S-4800 type). Technically, X-ray photoelectron spectroscopy (XPS, ULVAC-PHI, Inc., PHI 5000 VersaProbe III) was used to analyze the bonding between the electrolyte and electrode. The X-ray source for the measurement was monochromatic Al- $K\alpha$.

3. Results and Discussion

In this section, the ionic conductivity of solid electrolytes, the cycling performance of FIB cells, and the cycling fading cause were emphatically discussed. Furthermore, recent challenges of FIB cells for cycling fading were ascertained, and the detailed results of FIB experiments were outlined as follows.

3.1. Structure and ionic conductivity of $\text{La}_{0.9}\text{Ba}_{0.1}\text{F}_{2.9}$ electrolyte

The FE-SEM images of the LaF_3 precursor and $\text{La}_{0.9}\text{Ba}_{0.1}\text{F}_{2.9}$ samples are shown in Fig. 2. The $\text{La}_{0.9}\text{Ba}_{0.1}\text{F}_{2.9}$ electrolyte was prepared using the mechanical ball-milling method. Before milling, the size of the LaF_3 precursor was distributed at a range of 1–100 μm . After milling, nanoscale powders of the as-prepared $\text{La}_{0.9}\text{Ba}_{0.1}\text{F}_{2.9}$ were obtained. The particle size distribution was in the range of 100–300 nm. According to the energy-dispersive x-ray spectroscopy (EDS) analysis, the x value of $\text{La}_{1-x}\text{Ba}_x\text{F}_{3-x}$ was 0.109, as confirmed by the expected value ($x = 0.1$).

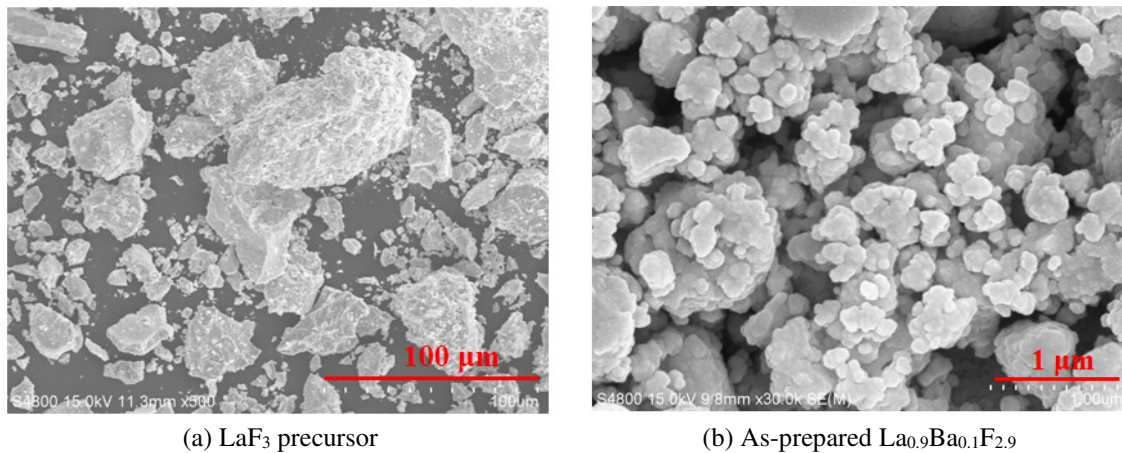


Fig. 2 FE-SEM images of LaF_3 precursor and $\text{La}_{0.9}\text{Ba}_{0.1}\text{F}_{2.9}$

Fig. 3 shows the XRD patterns of the LaF_3 precursor and as-prepared $\text{La}_{0.9}\text{Ba}_{0.1}\text{F}_{2.9}$ samples. The LaF_3 diffraction peaks at 24.195° (002), 24.763° (110), 27.614° (111), 43.602° (300), and 44.733° (113) shifted toward lower diffraction angles after mixing LaF_3 and BaF_2 by ball milling.

Such a finding indicates that LaF_3 was doped with Ba via ball milling. However, diffraction peaks of other impurities (e.g., BaF_2 and LaOF) were not observed in the XRD patterns. The BaF_2 doping LaF_3 was used to create fluoride vacancies to improve ionic mobility [1].

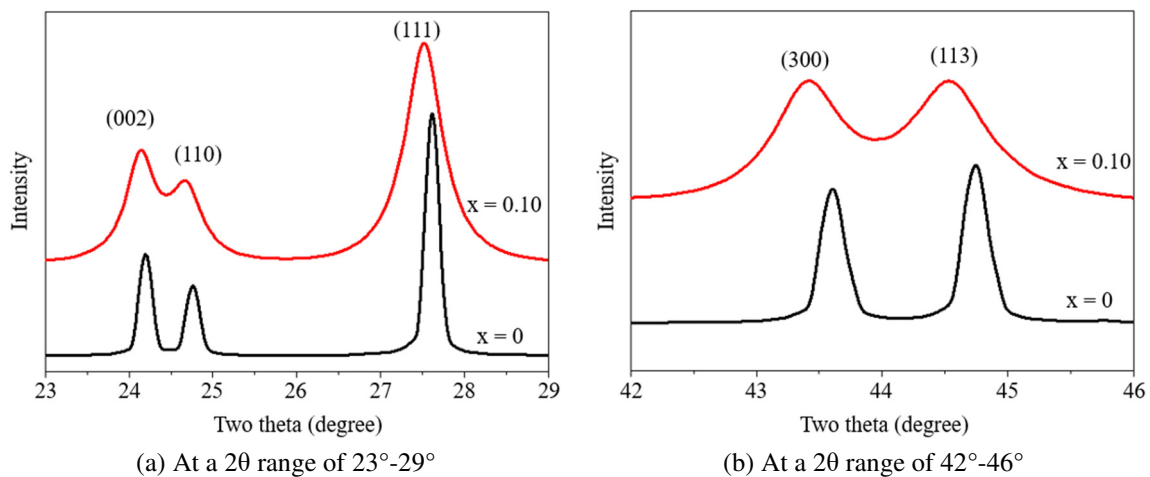


Fig. 3 XRD patterns of $\text{La}_{1-x}\text{Ba}_x\text{F}_{3-x}$ samples

To understand the crystallite composition of LaF_3 after Ba-doping, the lattice parameters a and c were calculated as follows:

Bragg's law [19]:

$$d = \frac{n\lambda}{2\sin\theta} \quad (6)$$

where d is lattice spacing (\AA), $n = 1$, λ is the X-ray wavelength (1.5406 \AA), and θ is peak position (in radians).

The structure of $\text{La}_{0.9}\text{Ba}_{0.1}\text{F}_{2.9}$ is hexagonally presented. The relationship between the lattice spacing and the lattice parameter can be described as [19]:

$$\frac{1}{d^2} = \frac{4}{3} \left(\frac{h^2 + hk + k^2}{a^2} \right) + \frac{l^2}{c^2} \quad (7)$$

where a and c are lattice parameters, and h , k , and l are Miller indices.

Rongeat et al. [9] reported that the cell parameters of a and c were 7.22 and 7.39 \AA for $\text{La}_{0.9}\text{Ba}_{0.1}\text{F}_{2.9}$ synthesis via the ball milling method. Bhatia et al. [10] developed a coprecipitation method to synthesize tysonite $\text{La}_{1-x}\text{Ba}_x\text{F}_{3-x}$ ($0 \leq x \leq 0.15$) solid electrolyte. The values of a and c were 7.225 and 7.397 \AA for the $\text{La}_{0.9}\text{Ba}_{0.1}\text{F}_{2.9}$ sample. As shown in Fig. 3(b), the lattice parameter, a , based on the (300) diffraction peak, was calculated using Eqs. (6) and (7). Similarly, the lattice parameter c was calculated based on the (002) diffraction peak. In this study, the values of a and c for LaF_3 were 7.184 and 7.350 \AA , respectively. After Ba doping through milling, the values of a and c were increased to 7.214 and 7.364 \AA , respectively. Similar values of a and c for the $\text{La}_{0.9}\text{Ba}_{0.1}\text{F}_{2.9}$ samples were obtained, compared to previous studies [9-10]. The aforementioned results bespeak the successful synthesis of $\text{La}_{0.9}\text{Ba}_{0.1}\text{F}_{2.9}$ using the ball milling method.

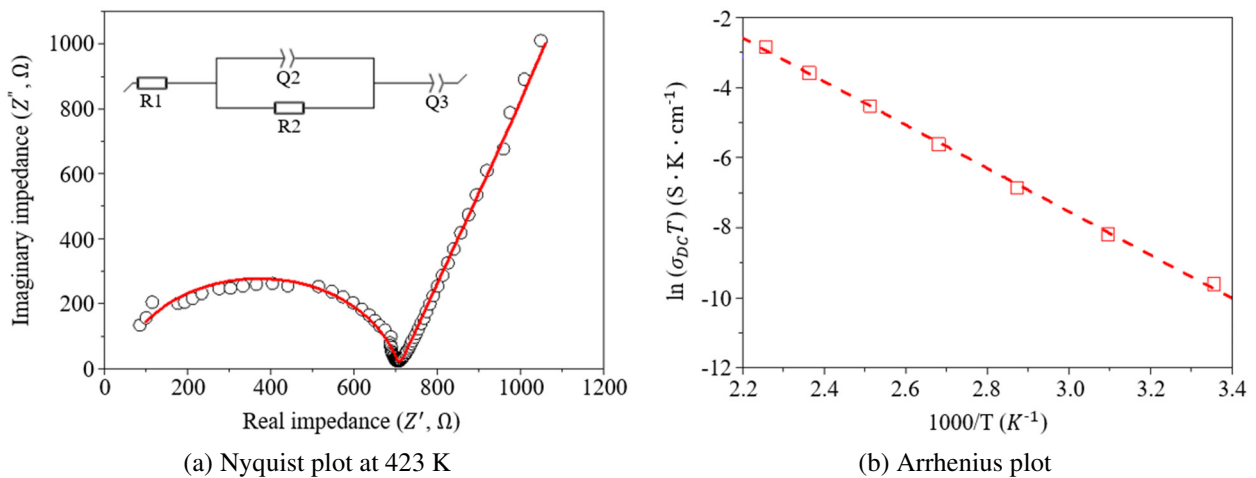


Fig. 4 Nyquist plot and Arrhenius plot of $\text{La}_{0.9}\text{Ba}_{0.1}\text{F}_{2.9}$

Table 1 lists the electrochemical parameters of $\text{La}_{0.9}\text{Ba}_{0.1}\text{F}_{2.9}$. The Nyquist plot and Arrhenius plot of the as-prepared $\text{La}_{0.9}\text{Ba}_{0.1}\text{F}_{2.9}$ were shown in Fig. 4. The ionic conductivities of the as-prepared $\text{La}_{0.9}\text{Ba}_{0.1}\text{F}_{2.9}$ sample were determined using EIS measurements. EIS spectra were recorded at a temperature range from 298 K to 443 K . The EIS spectra comprise a semicircle at a high frequency and a straight line at a low frequency, as shown in Fig. 4(a). The semicircular curve connotes that the conduction mechanism is dominated by the grain boundaries or bulk phenomena [11].

Table 1 Electrochemical parameters of $\text{La}_{0.9}\text{Ba}_{0.1}\text{F}_{2.9}$

Source	Method	T (K)	σ_{DC} (S/cm)	E_a (eV)
In this study	ball milling	423	6.6×10^{-5}	0.534
[6]	sol-gel	443	8.8×10^{-5}	0.531
[9]	ball milling	433	2.8×10^{-4}	0.550
[10]	coprecipitation	373	2.7×10^{-5}	0.560
[11]	ball milling	423	8.3×10^{-5}	-

Moreover, a straight line signifies the polarization of the electrode-electrolyte interface [10]. The total resistance of the $\text{La}_{0.9}\text{Ba}_{0.1}\text{F}_{2.9}$ samples was obtained by fitting the Nyquist plot to an equivalent circuit (as shown in the inset of Fig. 4(a) inset). R_1 , R_2 , Q_2 , and Q_3 correspond to the contact resistance, total resistance (bulk and grain boundaries), capacitance, and blocking electrodes, respectively [8]. In this study, the ionic conductivity (σ_{DC}) and activation energy (E_a) of $\text{La}_{0.9}\text{Ba}_{0.1}\text{F}_{2.9}$ by ball milling synthesis was 6.6×10^{-5} S/cm and 0.534 eV, respectively. Similar electrochemical parameters for $\text{La}_{0.9}\text{Ba}_{0.1}\text{F}_{2.9}$ have been reported previously [6, 9-11].

3.2. Cycling performance of solid-state FIB cell

The solid-state cell sample encompasses three layers: a cathode composite, an electrolyte, and an anode. Apropos the materials, the metal fluoride CuF_2 was applied as the active material within the cathode layer owing to its high theoretical capacity (527 mAh/g). Meanwhile, to improve CuF_2 conductivity, conductive additives such as carbon black and $\text{La}_{0.9}\text{Ba}_{0.1}\text{F}_{2.9}$ were used herein. The $\text{La}_{0.9}\text{Ba}_{0.1}\text{F}_{2.9}$ with ionic conductivity of 6.6×10^{-5} S/cm at 423 K was used as the electrolyte layer in the cell. Two elements, Sn and Pb, were tested in the cell experiments. Two cathode/electrolyte/anode cell types are denoted as $\text{CuF}_2/\text{La}_{0.9}\text{Ba}_{0.1}\text{F}_{2.9}/\text{Sn}$ and $\text{CuF}_2/\text{La}_{0.9}\text{Ba}_{0.1}\text{F}_{2.9}/\text{Pb}$.

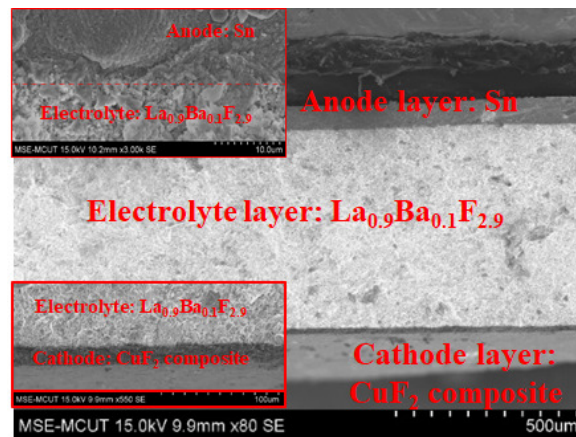


Fig. 5 Cross-sectional FE-SEM image of $\text{CuF}_2/\text{La}_{0.9}\text{Ba}_{0.1}\text{F}_{2.9}/\text{Sn}$ cell

Fig. 5. depicts the cross-sectional FE-SEM images of the $\text{CuF}_2/\text{La}_{0.9}\text{Ba}_{0.1}\text{F}_{2.9}/\text{Sn}$ cell. The thickness of the cathode, electrolyte, and anode layers were 10 μm , 550 μm , and 100 μm , respectively. The total thickness of the cell was approximately 660 μm , approximating the previously reported values [8, 11]. The FE-SEM image also shows that both the anode and cathode layers were uniformly attached to the $\text{La}_{0.9}\text{Ba}_{0.1}\text{F}_{2.9}$ electrolyte layer. A similar cross-sectional FE-SEM image for the $\text{CuF}_2/\text{La}_{0.9}\text{Ba}_{0.1}\text{F}_{2.9}/\text{Pb}$ cell is obtained.

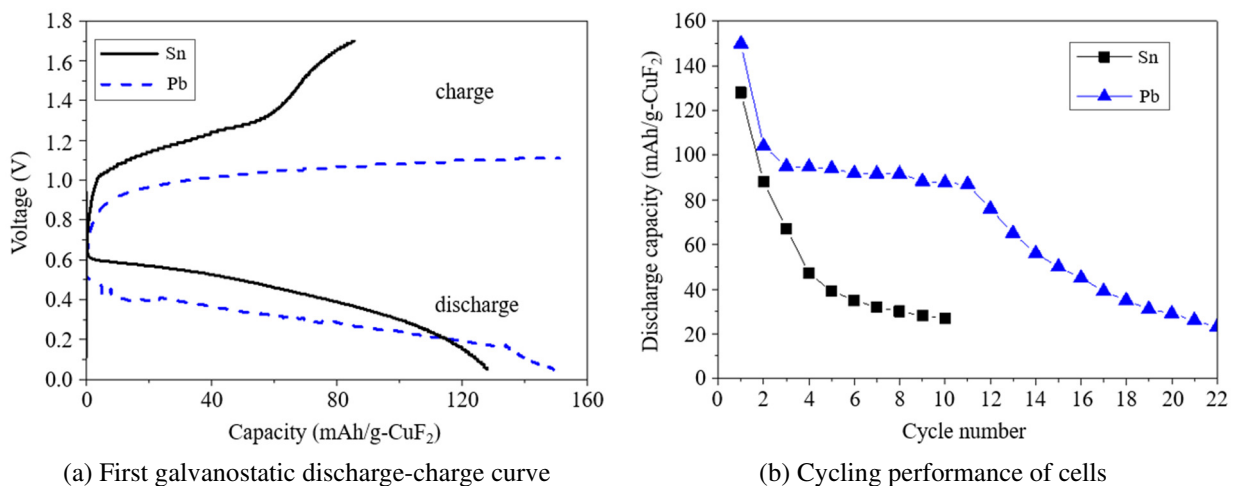


Fig. 6 Electrochemical studies of cells with different anode materials

Fig. 6 illustrates the discharge–charge curves and cycling performance of the cells with different anode materials. As shown in Fig. 6(a), the open-circuit voltage (OCV) of $\text{CuF}_2/\text{La}_{0.9}\text{Ba}_{0.1}\text{F}_{2.9}/\text{Sn}$ stood at 0.69 V. The first discharge capacity was 128 mAh/g- CuF_2 at 423 K and under $40 \mu\text{A}/\text{cm}^2$. Meanwhile, only 24% of the theoretical capacity of CuF_2 (527 mAh/g) was obtained. Such a result symbolizes the incomplete conversion of CuF_2 to Cu. Compared with the $\text{CuF}_2/\text{La}_{0.9}\text{Ba}_{0.1}\text{F}_{2.9}/\text{Pb}$ cell, the first discharge capacity was 150 mAh/g- CuF_2 , which is 28% of the theoretical capacity. Similar first discharge capacities were found with either Sn or Pb as anode materials. Reddy and Fichtner [7] developed the $\text{CuF}_2/\text{La}_{0.9}\text{Ba}_{0.1}\text{F}_{2.9}/\text{Ce}$ cell that could achieve 322 mAh/g (61% of theoretical capacity) for the first discharge at 423K with a current density of $10 \mu\text{A}/\text{cm}^2$.

Thieu et al. [14] discovered that the first discharge capacity of 360 mAh/g (68% of theoretical capacity) was measured for $\text{CuF}_2/\text{La}_{0.9}\text{Ba}_{0.1}\text{F}_{2.9}/\text{La}$ cell at 423 K and under a current density of 4 mA/g (approached to $10 \mu\text{A}/\text{cm}^2$). Furthermore, the first discharge capacity of 331 mAh/g for the $\text{CuF}_2/\text{La}_{0.9}\text{Ba}_{0.1}\text{F}_{2.9}/\text{Sn}$ cell under the current density of $10 \mu\text{A}/\text{cm}^2$ was also obtained. Therefore, the susceptibility of discharge capacities can be further attested by current density, which may be attributed to the interfacial resistance of the electrode and electrolyte in the solid-state cells. The cycling performances of the $\text{CuF}_2/\text{La}_{0.9}\text{Ba}_{0.1}\text{F}_{2.9}/\text{Sn}$ and $\text{CuF}_2/\text{La}_{0.9}\text{Ba}_{0.1}\text{F}_{2.9}/\text{Pb}$ cells are shown in Fig. 6(b). The cycling stability of $\text{CuF}_2/\text{La}_{0.9}\text{Ba}_{0.1}\text{F}_{2.9}/\text{Sn}$ cell was lower than that of $\text{CuF}_2/\text{La}_{0.9}\text{Ba}_{0.1}\text{F}_{2.9}/\text{Pb}$ cell. The discharge capacity of the cell with Sn anode plunged from 128 mAh/g (first cycle) to 28 mAh/g (tenth cycle). In contrast, stable cycling of $\text{CuF}_2/\text{La}_{0.9}\text{Ba}_{0.1}\text{F}_{2.9}/\text{Pb}$ cell, maintained at 90 mAh/g, was obtained before 10 discharge–charge cycles. Unfortunately, after the 11th cycle, the discharge capacity gradually decreased to approximately 23 mAh/g (the 22th cycle).

3.3. XPS analysis of cells before and after cycling

To clarify the causes of cycling fading, the anode layer of the cell was studied after manifold cycles. The XPS profiles of the cells with different anode materials after cycling are shown in Fig. 7. Concerning the as-prepared cell with Sn anode case, two peaks of Sn 3d5/2 and Sn 3d3/2 situated at 484.6 eV and 493.0 eV of Sn^0 in Sn, respectively [20]. The other peaks at 485.9 eV and 494.6 eV of Sn^{2+} in SnO [21] were also found owing to air oxidation during XPS sample preparation. After the first discharge, the Sn 3d peaks shifted to 487.3 eV (Sn 3d5/2) and 495.7 eV (Sn 3d5/2), which implied the SnF_2 formation [22]. After 10 cycles, a peak at 488.4 eV (Sn 3d5/2) for Sn^{4+} in SnF_4 was observed [23]. The XPS results indicate that Sn easily forms Sn(IV)F_4 with high binding energy after several fluoridation/defluorination reactions. The poor cycling of $\text{CuF}_2/\text{La}_{0.9}\text{Ba}_{0.1}\text{F}_{2.9}/\text{Sn}$ cell can be attributed to the irreversible Sn(IV)F_4 formation during cycling at 423 K.

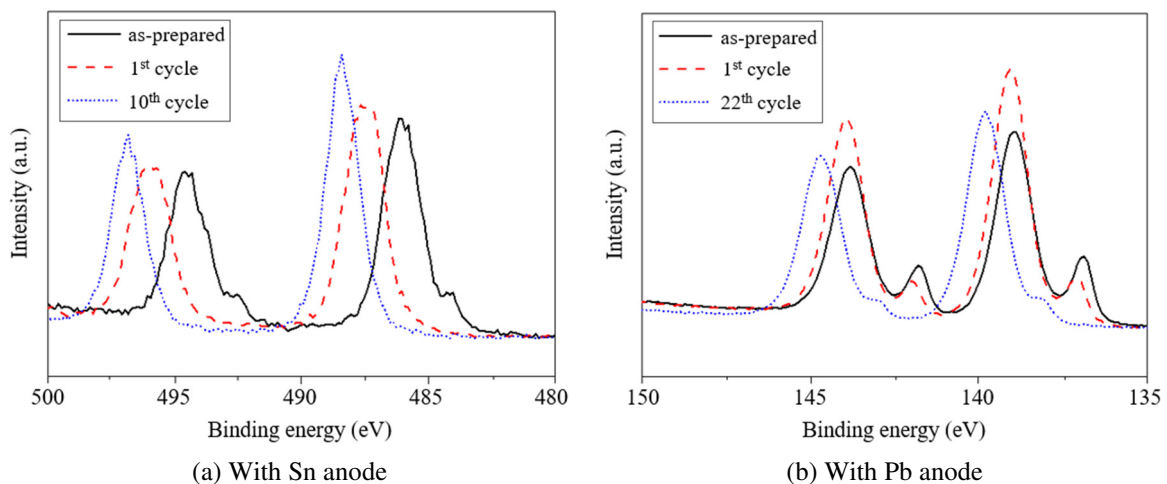


Fig. 7 XPS spectra of the cell with different anode materials

Regarding the as-prepared cell with Pb anode case, the Pb(II)O peaks at 138.8 eV (Pb 4f 7/2) and 143.6 eV (Pb 4f 5/2) accompanied by Pb^0 peaks at 136.9 eV (Pb 4f 7/2) and 141.6 eV (Pb 4f 5/2), were found [24]. After the first cycle, the binding energy of XPS peaks (Pb 4f 7/2 and Pb 4f 5/2) slightly increased to 139.0 eV and 144.0 eV, corresponding to Pb(II)F_2 [25].

Thus, the anode of Pb^0 was converted to Pb^{2+} (PbF_2) during the fluoridation reaction (cell discharge). Notably, the Pb 4f peaks at 139.8 eV (Pb 4f 7/2) and 144.7 eV (Pb 4f 5/2) were determined after twenty-two cycles, corresponding to the Pb complex with high valency (e.g., Pb(IV)F_4) [26].

3.4. Summary of FIB cell cycling technology challenges

Table 2 enumerates the common fading problem for the solid-state FIB cell. According to previous studies [7-8, 14, 26-27], the large volume change of active materials increased the interface resistance of electrode/electrolyte during the cycling of fluoridation/defluorination reaction. The physical contact between the active material, carbon black, $\text{La}_{0.9}\text{Ba}_{0.1}\text{F}_{2.9}$, and the layer contact between the electrode and the electrolyte was a major hindrance to the cycling performance of solid-state FIB cells [7-8, 27]. In addition, the irreversible material formation (e.g., LaOF and CF_x) was causally important for cycling fading [14, 26]. In this study, the Sn and Pb metals were used as the anode material for the solid-state FIB cell. The reversible materials for Sn(II)F_2 and Pb(II)F_2 formation were demonstrated after the fluoridation reaction (cell discharge). After several discharge-charge cycles, Sn(IV)F_4 and Pb(IV)F_4 were formed, which might incur cycling deterioration.

Table 2 Summary of solid-state FIB cell fading

Sources	Cathode/Electrolyte/Anode	T (K)	Current density ($\mu\text{A}/\text{cm}^2$)	Cycles	Causes of fading
In this study	$\text{CuF}_2/\text{La}_{0.9}\text{Ba}_{0.1}\text{F}_{2.9}/\text{Sn}$	423	40	10	The anode Sn^0 converts to form irreversible Sn(IV) fluoride during the cycling.
	$\text{CuF}_2/\text{La}_{0.9}\text{Ba}_{0.1}\text{F}_{2.9}/\text{Pb}$			22	The anode Pb^0 converts to form an irreversible Pb(IV) complex during the cycling.
[7]	$\text{CuF}_2/\text{La}_{0.9}\text{Ba}_{0.1}\text{F}_{2.9}/\text{Ce}$	423	10	-	The volume change weakens the electrode-electrolyte contact.
	$\text{BiF}_3/\text{La}_{0.9}\text{Ba}_{0.1}\text{F}_{2.9}/\text{Ce}$			38	
[8]	$\text{BiF}_3/\text{BaSnF}_4/\text{Sn}$	298-423	10	10	The increase in cell resistance was owing to the increase in the particle size of the Sn anode during cycling.
[14]	$\text{CuF}_2/\text{La}_{0.9}\text{Ba}_{0.1}\text{F}_{2.9}/\text{La}$	423	10	23	LaOF irreversibly formed at the anode/electrolyte interface. Cu diffuses into the electrolyte at the cathode/electrolyte interface.
[26]	-	-	-	-	The electrochemical properties of the cell were faded by the insulative CF_x formation.
[27]	$\text{BiF}_3/\text{Ba}_{0.98}\text{Nd}_{0.02}\text{SnF}_{4.02}/\text{Sn}$	298	10	20	The volume change of electrode materials and increase in the electrode-electrolyte interface resistance during the cycling.

4. Conclusions

In this study, the cycling performance of solid-state FIB cells with different anode materials (Sn and Pb) was investigated. The cathode and solid electrolyte were CuF_2 composite and $\text{La}_{0.9}\text{Ba}_{0.1}\text{F}_{2.9}$ with ionic conductivity of $6.6 \times 10^{-5} \text{ S/cm}$ (at 423 K), respectively. Apropos the environment, all cycling experiments were performed at 423 K and under $40 \mu\text{A}/\text{cm}^2$. The electrochemical measurements indicate that the cycling stability of the $\text{CuF}_2/\text{La}_{0.9}\text{Ba}_{0.1}\text{F}_{2.9}/\text{Pb}$ cell is higher than that of the $\text{CuF}_2/\text{La}_{0.9}\text{Ba}_{0.1}\text{F}_{2.9}/\text{Sn}$ cell. The first and tenth discharge capacities of 150 mAh/g and 90 mAh/g, respectively, were obtained for the $\text{CuF}_2/\text{La}_{0.9}\text{Ba}_{0.1}\text{F}_{2.9}/\text{Pb}$ cell. On the other hand, the first and tenth discharge capacities of 128 mAh/g and 27 mAh/g were obtained for the $\text{CuF}_2/\text{La}_{0.9}\text{Ba}_{0.1}\text{F}_{2.9}/\text{Sn}$ cell. According to the XPS analysis, the cycling fading for the FIB cells could be attributed to the high valence number of metal fluorides (e.g., Sn(IV)F_4 and Pb(IV)F_4). The resultant finding indicates that Sn and Pb as anode materials were unfavorable under high-temperature conditions (e.g., 423 K) for the discharge/charge cycling of FIB cells. The development of an advanced solid electrolyte with high conductivity at room temperature would be the decisive factor in future work for improving FIB applicability and reducing the demand for electrode materials screening.

Acknowledgments

This work gratefully acknowledges the financial support from the National Science and Technology Council, Taiwan, ROC (MOST 111-3111-Y-042A-008).

Conflicts of Interest

The authors declare no conflict of interest.

References

- [1] M. A. Nowroozi, I. Mohammad, P. Molaiyan, K. Wissel, A. R. Munnangi, and O. Clemens, "Fluoride Ion Batteries – Past, Present, and Future," *Journal of Materials Chemistry A*, vol. 9, no. 10, pp. 5980-6012, March 2021.
- [2] A. Vamsi, J. Ansari, S. Mk, C. Pany, B. John, A. Samridh, et al., "Structural Design and Testing of Pouch Cells," *Journal of Energy Systems*, vol. 5, no. 2, pp. 80-91, June 2021.
- [3] M. S. Alam, R. K. Pillai, and N. Murugesan, *Developing Charging Infrastructure and Technologies for Electric Vehicles*, Hershey PA: Engineering Science Reference, pp. 156-177, 2022.
- [4] L. Liu, L. Yang, M. Liu, X. Li, D. Shao, K. Luo, et al., "SnF₂-Based Fluoride Ion Electrolytes MSnF₄ (M = Ba, Pb) for the Application of Room-Temperature Solid-State Fluoride Ion Batteries," *Journal of Alloys and Compounds*, vol. 819, article no. 152983, April 2020.
- [5] C. Pany and G. Li, "Editorial: Application of Periodic Structure Theory With Finite Element Approach," *Frontiers in Mechanical Engineering*, vol. 9, article no. 1192657, 2023.
- [6] L. Zhang, M. A. Reddy, and M. Fichtner, "Development of Tysonite-Type Fluoride Conducting Thin Film Electrolytes for Fluoride Ion Batteries," *Solid State Ionics*, vol. 272, pp. 39-44, April 2015.
- [7] M. A. Reddy and M. Fichtner, "Batteries Based on Fluoride Shuttle," *Journal of Materials Chemistry*, vol. 21, no. 43, pp. 17059-17062, November 2011.
- [8] I. Mohammad, R. Witter, M. Fichtner, and M. A. Reddy, "Room-Temperature, Rechargeable Solid-State Fluoride-Ion Batteries," *ACS Applied Energy Materials*, vol. 1, no. 9, pp. 4766-4775, September 2018.
- [9] C. Rongeat, M. A. Reddy, R. Witter, and M. Fichtner, "Solid Electrolytes for Fluoride Ion Batteries: Ionic Conductivity in Polycrystalline Tysonite-Type Fluorides," *ACS Applied Materials & Interfaces*, vol. 6, no. 3, pp. 2103-2110, February 2014.
- [10] H. Bhatia, D. T. Thieu, A. H. Pohl, V. S. K. Chakravadhanula, M. H. Fawey, C. Kübel, et al., "Conductivity Optimization of Tysonite-Type La_{1-x}Ba_xF_{3-x} Solid Electrolytes for Advanced Fluoride Ion Battery," *ACS Applied Materials & Interfaces*, vol. 9, no. 28, pp. 23707-23715, July 2017.
- [11] I. Mohammad, R. Witter, M. Fichtner, and M. A. Reddy, "Introducing Interlayer Electrolytes: Toward Room-Temperature High-Potential Solid-State Rechargeable Fluoride Ion Batteries," *ACS Applied Energy Materials*, vol. 2, no. 2, pp. 1553-1562, February 2019.
- [12] F. Preishuber-Pflügl, V. Epp, S. Nakhil, M. Lerch, and M. Wilkening, "Defect-Enhanced F⁻ Ion Conductivity in Layer-Structured Nanocrystalline BaSnF₄ Prepared by High-Energy Ball Milling Combined With Soft Annealing," *Physica Status Solidi (C)*, vol. 12, no. 1-2, pp. 10-14, January 2015.
- [13] J. Wang and C. Ma, "Superior Room-Temperature Cycling Stability of Fluoride-Ion Batteries Enabled by Solid Electrolytes Synthesized by the Solid-State Reaction," *Science China Materials*, vol. 65, no. 11, pp. 3025-3032, November 2022.
- [14] D. T. Thieu, M. H. Fawey, H. Bhatia, T. Diemant, V. S. K. Chakravadhanula, R. J. Behm, et al., "CuF₂ As Reversible Cathode for Fluoride Ion Batteries," *Advanced Functional Materials*, vol. 27, no. 31, article no. 1701051, August 2017.
- [15] M. A. Nowroozi, K. Wissel, M. Donzelli, N. Hosseinpourkahvaz, S. Plana-Ruiz, U. Kolb, et al., "High Cycle Life All-Solid-State Fluoride Ion Battery With La₂NiO_{4+d} High Voltage Cathode," *Communications Materials*, vol. 1, article no. 27, 2020.
- [16] L. Zhang, M. A. Reddy, and M. Fichtner, "Electrochemical Performance of All Solid-State Fluoride-Ion Batteries Based on Thin-Film Electrolyte Using Alternative Conductive Additives and Anodes," *Journal of Solid State Electrochemistry*, vol. 22, no. 4, pp. 997-1006, April 2018.
- [17] J. Liu, L. Yi, X. Chen, D. Li, S. Ni, J. Xia, et al., "Studies on Fluoride Ion Conductivity of the Mechanochemically Synthesized β -KSbF₄ for All-Solid-State Fluoride-Ion Batteries," *Sustainable Materials and Technologies*, vol. 39, article no. e00810, April 2024.

- [18] Y. Yu, M. Lei, D. Li, and C. Li, "Near-Room-Temperature Quasi-Solid-State F-Ion Batteries With High Conversion Reversibility Based on Layered Structured Electrolyte," *Advanced Energy Materials*, vol. 13, no. 12, article no. 2203168, March 2023.
- [19] B. D. Cullity, *Elements of X-Ray Diffraction*, Pearson New International Edition, 3rd ed., United Kingdom: Pearson, 2014.
- [20] A. Wiczorek, H. Lai, J. Pious, F. Fu, and S. Siol, "Resolving Oxidation States and X-site Composition of Sn Perovskites Through Auger Parameter Analysis in XPS," *Advanced Materials Interfaces*, vol. 10, no. 7, article no. 2201828, March 2023.
- [21] P. C. Hsu, C. J. Hsu, C. H. Chang, S. P. Tsai, W. C. Chen, H. H. Hsieh, et al., "Sputtering Deposition of P-type SnO Films with SnO₂ Target in Hydrogen-Containing Atmosphere," *ACS Applied Materials & Interfaces*, vol. 6, no. 16, pp. 13724-13729, August 2014.
- [22] J. Liu, L. Yi, P. Zeng, C. Zou, X. Chen, X. Tao, et al., "Point Defect Engineering Enabled the High Ionic Conductivity of BaSnF₄ for Solid-State Fluoride-Ion Batteries at Room Temperature," *Energy & Fuels*, vol. 36, no. 24, pp. 15258-15267, December 2022.
- [23] M. Senna, E. Turianicová, V. Sepelák, M. Bruns, G. Scholz, S. Lebedkin, et al., "Fluorine Incorporation Into SnO₂ Nanoparticles by Co-milling With Polyvinylidene Fluoride," *Solid State Sciences*, vol. 30, pp. 36-43, April 2014.
- [24] H. Cai, Y. Sun, X. Zhang, L. Zhang, H. Liu, Q. Li, et al., "Reduction Temperature-Dependent Nanoscale Morphological Transformation and Electrical Conductivity of Silicate Glass Microchannel Plate," *Materials*, vol. 12, no. 7, article no. 1183, April 2019.
- [25] H. Konishi, T. Minato, T. Abe, and Z. Ogumi, "Charge and Discharge Reactions of a Lead Fluoride Electrode in a Liquid-Based Electrolyte for Fluoride Shuttle Batteries:-The Role of Triphenylborane as an Anion Acceptor-," *ChemistrySelect*, vol. 4, no. 19, pp. 5984-5987, May 2019.
- [26] A. Grenier, A. G. Porras-Gutierrez, M. Body, C. Legein, F. Chrétien, E. Raymundo-Piñero, et al., "Solid Fluoride Electrolytes and Their Composite With Carbon: Issues and Challenges for Rechargeable Solid State Fluoride-Ion Batteries," *The Journal of Physical Chemistry C*, vol. 121, no. 45, pp. 24962-24970, November 2017.
- [27] L. Liu, L. Yang, D. Shao, K. Luo, C. Zou, Z. Luo, et al., "Nd³⁺ Doped BaSnF₄ Solid Electrolyte for Advanced Room-Temperature Solid-State Fluoride Ion Batteries," *Ceramics International*, vol. 46, no. 12, pp. 20521-20528, August 2020.



Copyright© by the authors. Licensee TAETI, Taiwan. This article is an open-access article distributed under the terms and conditions of the Creative Commons Attribution (CC BY-NC) license (<https://creativecommons.org/licenses/by-nc/4.0/>).